# 9

#### Research article

Hongwei Zhao<sup>a,\*</sup>, Ran Zhang<sup>a</sup>, Hamid T. Chorsi<sup>a</sup>, Wesley A. Britton, Yuyao Chen, Prasad P. Iyer, Jon A. Schuller, Luca Dal Negro and Jonathan Klamkin

# Gate-tunable metafilm absorber based on indium silicon oxide

https://doi.org/10.1515/nanoph-2019-0190 Received June 20, 2019; revised August 9, 2019; accepted August 21, 2019

**Abstract:** In this work, reconfigurable metafilm absorbers based on indium silicon oxide (ISO) were investigated. The metafilm absorbers consist of nanoscale metallic resonator arrays on metal-insulator-metal (MIM) multilayer structures. The ISO was used as an active tunable layer embedded in the MIM cavities. The tunable metafilm absorbers with ISO were then fabricated and characterized. A maximum change in the reflectance of 57% and up to 620 nm shift in the resonance wavelength were measured.

**Keywords:** metafilm; indium silicon oxide; metamaterials; metasurface.

## 1 Introduction

Light can be strongly coupled at a metal-dielectric interface, enabling subwavelength optical components that overcome the diffraction limit [1]. Metasurfaces or

<sup>a</sup>Hongwei Zhao, Ran Zhang and Hamid T. Chorsi: These authors equally contributed to this work.

Ran Zhang and Wesley A. Britton: Division of Material Science and Engineering, Boston University, Brookline, MA 02446, USA Hamid T. Chorsi, Prasad P. Iyer, Jon A. Schuller and Jonathan Klamkin: Electrical and Computer Engineering Department, University of California, Santa Barbara, CA 93106, USA Yuyao Chen: Department of Electrical and Computer Engineering and Photonics Center, Boston University, Boston, MA 02215, USA Luca Dal Negro: Division of Material Science and Engineering, Boston University, Brookline, MA 02446, USA; Department of Electrical and Computer Engineering and Photonics Center, Boston University, Boston, MA 02215, USA; and Department of Physics, Boston University, Boston, MA 02215, USA

metafilms consist of subwavelength or nano-scale artificial metallic resonators, such as metal stripes, nano rods or Mie resonators, thus allowing for the manipulation of the light amplitude, phase and polarization [2–4]. In the past decade, reconfigurable metasurfaces have been investigated for a wide range of applications, including optical antenna, optical modulation, beam steering, solar cells, light detection and bio-sensing [5–11]. To enable active tuning, electro-optical tunable materials are incorporated into metasurfaces. By embedding tunable materials in metal-insulator-metal (MIM) plasmonic cavities, the optical properties of light waves can be tuned with a gate bias. Tunable materials, such as graphene, transparent conductive oxides (TCOs), highly doped III-V semiconductors and metal nitrides have been investigated [12–18].

TCOs have drawn significant attention due to their fabrication simplicity and significant electrical tunability in the near- and mid-IR wavelength ranges. TCOs are transparent in the visible range owing to their large bandgap. They demonstrate dielectric- or metal-like optical properties depending on the carrier doping concentration. TCOs like indium tin oxide (ITO), aluminum-doped ZnO (AZO), and gallium-doped ZnO (GZO) have been widely investigated. In those works, the complex refractive index of TCOs was actively tuned by field-effect modulation within MIM plasmonic cavities, resulting in control of light transmission and reflection. Electrically gated amplitude and phase control opens the path to applications in high-speed efficient optical modulation and dynamic beam steering [19–25].

Gate-tunable metasurfaces based on ITO have been reported for engineering light amplitude and phase [26–31]. As an alternative TCO, indium silicon oxide (ISO) is a good candidate for a transparent electrode, for flexible organic solar cells and for thin-film transistors [32–35]. Silicon doping has been reported to increase the Hall mobility and reduce the carrier concentration compared with tin in indium oxide (In<sub>2</sub>O<sub>3</sub>) [36]. Very recently, plasmonic responses have been demonstrated in ISO thin films, making ISO a promising novel material

<sup>\*</sup>Corresponding author: Hongwei Zhao, Electrical and Computer Engineering Department, University of California, Santa Barbara, CA 93106, USA, e-mail: hwzhao@ece.ucsb.edu. https://orcid.org/0000-0002-7623-9558

platform for metaphotonic applications. Moreover, the Sicompatibility of the ISO material and its wide tunability of the screened plasma frequency across the mid-IR spectrum provide additional degrees of freedom for device engineering [37, 38]. In the current work, we experimentally studied metafilm absorbers based on ISO. The amplitude of the reflected light was actively tuned with a gate bias. A maximum change in the reflectance of 57% and up to 620 nm shift in the resonance wavelength were measured.

### 2 Metasurfaces based on ISO

#### 2.1 Device fabrication

As shown in Figure 1, the metafilm absorber consists of a metallic reflecting substrate, a 20 nm-thick ISO film, a 40 nm-thick hafnium dioxide (HfO $_2$ ) film and 50 nm-thick metallic resonator arrays. The resonator arrays are formed with interdigitated sub-wavelength gold (Au) rods that are connected to metal traces. Figure 1B describes the device operating principle whereby the underlying Au reflecting layer is connected to the ground and a bias voltage (V) is applied to the MIM cavity. The resonator arrays are designed with a fixed period (P) of 1  $\mu$ m but different widths (W) for each of the three primary device geometries. The near-normal incidence TE-polarized light (the in-plane electrical field is perpendicular to the long axis of the resonator) resonantly couples to the surface plasmons. The resonance wavelength and effective index

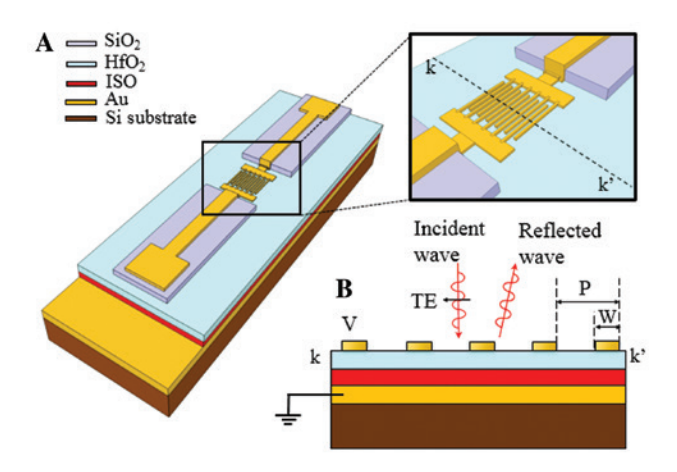


**Figure 1:** The gate-tunable metafilm absorber based on ISO. (A) 3D schematic of the metafilm absorber. (B) Cross section of the multi-layer structure describing operating principles.

of the plasmonic modes depend on the permittivity of the ISO layer and the geometry of the metallic resonators.

To fabricate the devices, first, a reflecting metal stack of 5 nm titanium (Ti) and 100 nm Au was deposited onto a silicon (Si) substrate. The ISO thin film was sputterdeposited onto the metallic reflecting substrate, using an Angstrom EvoVac system via the code position of an In<sub>2</sub>O<sub>2</sub> target (99.99% purity) and a SiO, target (99.99% purity) [37]. Then, a HfO<sub>2</sub> dielectric layer was deposited using atomic layer deposition (ALD). The Au resonator arrays were fabricated on top of the HfO, using electron beam lithography and metal lift-off. A 600 nm-thick SiO, layer was deposited using electron-beam evaporation and patterned with a lift-off process. On top of the silicon dioxide (SiO<sub>2</sub>) layer, metal pads comprising 15 nm-thick Ti and 50 nm-thick Au layers were deposited. Finally, the HfO, and ISO layers were patterned and etched to expose the lower reflecting metal layer for electrical contact. The microscope images of the fabricated metafilm absorbers are shown in Figure 2. In this work, three devices that have the same period P=1.0 µm but with different widths were investigated: D1 (W=300 nm), D2 (W=405 nm) and D3 (W = 850 nm).

#### 2.2 Material model

The dielectric permittivity of ISO can be described by the Drude model given by

$$\varepsilon = \varepsilon_r + i\varepsilon_i = \varepsilon_\infty - \frac{\omega_p^2}{(\omega^2 + i\Gamma\omega)},\tag{1}$$

where  $\varepsilon_{\infty}$  is the infinite frequency permittivity,  $\Gamma$  is the collision frequency and  $\omega_p$  is the plasma frequency, which depends on the carrier concentration (N) and electron effective mass ( $m^*$ ) according to the following:

$$\omega_p^2 = \frac{Ne^2}{m^* \varepsilon_o},\tag{2}$$

where e is the elementary charge and  $\varepsilon_0$  is the vacuum permittivity. The permittivity of the ISO thin film measured with ellipsometery (MIR J. A. Woollam VASE) is plotted in Figure 3.

Several advantages of the ISO platform are related to its large mobility for improved device response time [33], its significantly reduced surface roughness at larger thicknesses for improved device fabricability [37] and

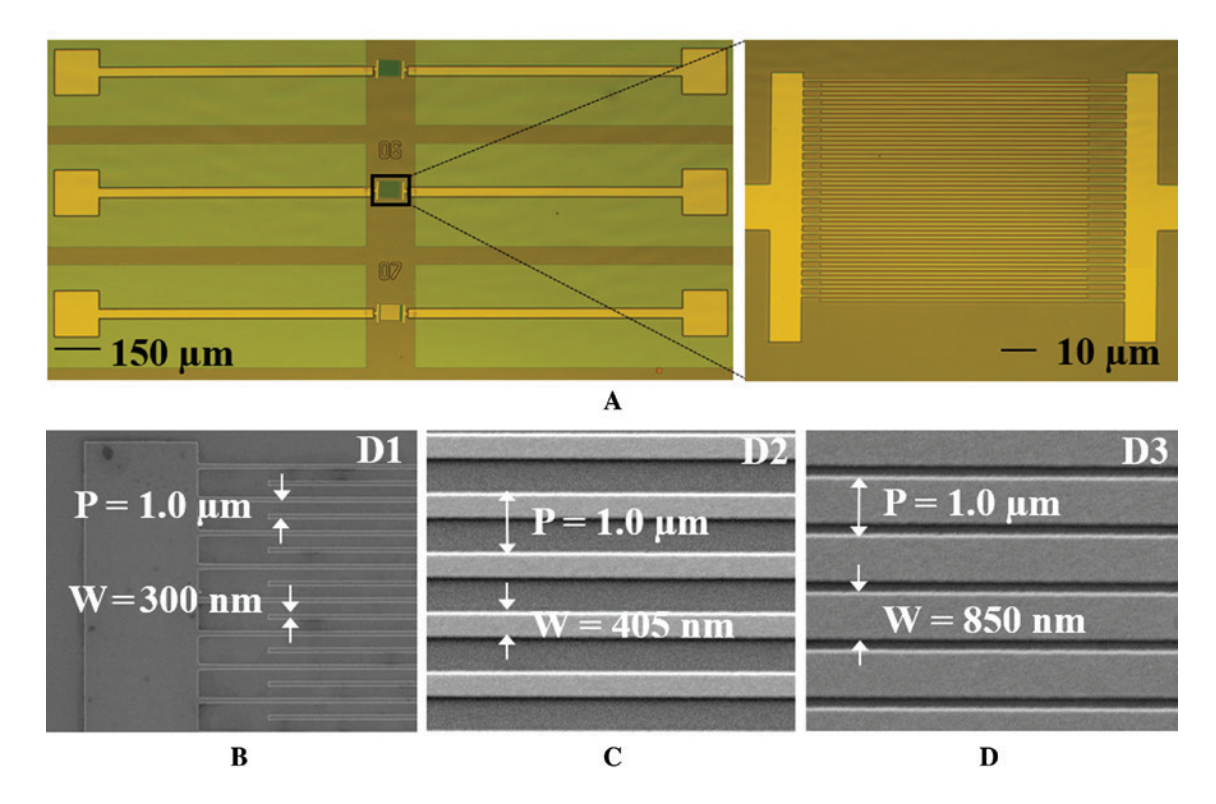


Figure 2: Fabricated metafilm absorbers.

(A) The optical microscope images of the fabricated metafilm absorbers. (B-D) Close up scanning electron microscope images of the devices with metal rod widths of 300, 405 and 850 nm.

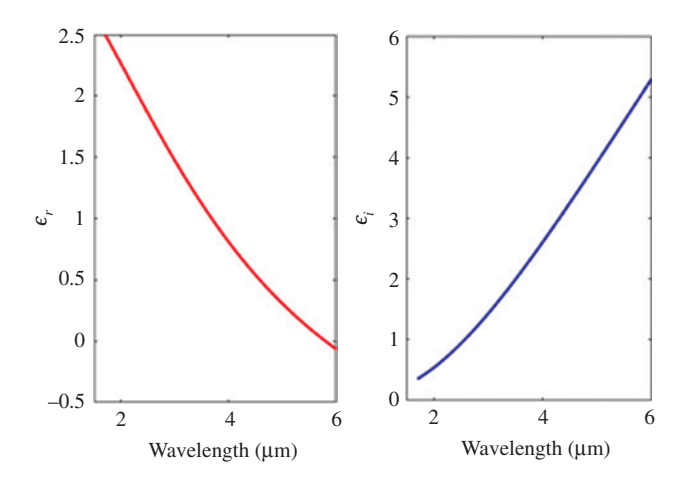
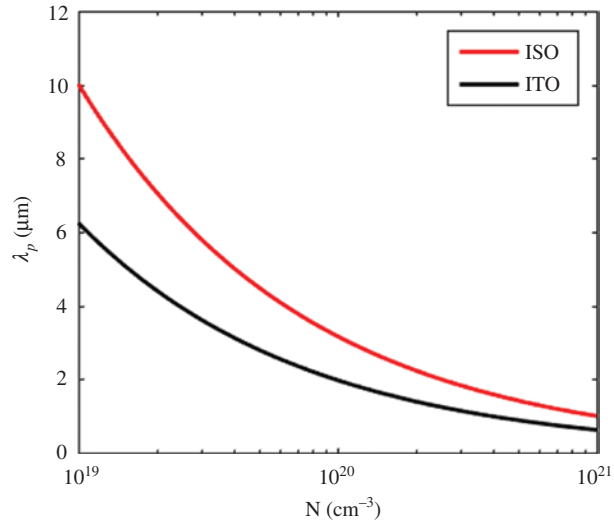


Figure 3: The permittivity of the ISO thin film.

its engineering potential for mid-IR localized plasmon resonances, which allow active device applications [37]. Specifically, we will now elaborate on the advantages on ISO as a novel epsilon-near-zero (ENZ) tunable material for optical modulation.

Optical modulation in MIM TCO devices is driven by the accumulation and depletion of free charge carriers. Likewise, the optical constants of TCO materials can be



**Figure 4:**  $\lambda_p$  as a function of *N* for both ITO and ISO with an electron effective mass  $(m^*)$  of  $m^* = 0.35 m_a$  and  $m^* = 0.90 m_a$ , respectively.

modeled using the Drude model at the wavelengths of interest.

Equation 3 defines the plasma wavelength  $(\lambda_n)$  under the assumption of parabolic bands with the free charge carrier effective mass  $(m^*)$  that is inversely proportional

to the band curvature. Equation 4 is the classical Drude model assuming no high frequency contributions to the dispersion or damping due to collisions. Under these conditions, when the wavelength equals  $\lambda_n$ , the material permittivity will be equal to zero.

$$\lambda_p \equiv 2\pi c \sqrt{\frac{m^* \varepsilon_0}{Ne^2}} \tag{3}$$

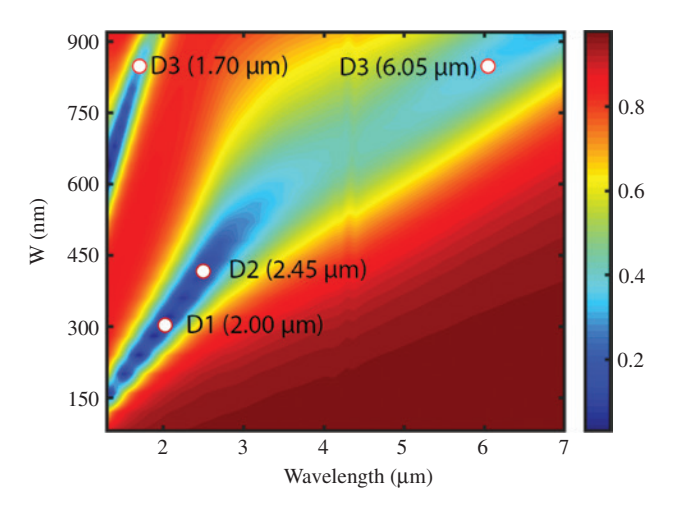


Figure 5: The simulated reflectance spectrum map for a resonator period of 1.0 µm as a function of wavelength and width of the resonator rod.

The resonance wavelengths corresponding to the widths for devices D1, D2, and D3 are marked.

$$\varepsilon_r(\lambda) = 1 - \left(\frac{\lambda}{\lambda_p}\right)^2 \tag{4}$$

Using ellipsometry and the Hall effect measurement technique, we have measured the screened plasma frequency  $(\omega_n)$  and N of the ISO material integrated into our presented devices. The ISO materials' optical constants are well described by the Drude model; therefore,  $m^*$  can be estimated using these values. We observed  $\omega_n = 1.06 \times 10^{15} \text{ rad/s}$  and  $N = 3.2 \times 10^{20} \text{ cm}^{-3}$  after a 250°C vacuum annealing step, which yields an effective mass of  $m^* = 0.9 \, m_o$ . This is about three times larger than the typical value of ITO, which is  $m^* = 0.35 m_e$ .

Figure 4 illustrates the plasma wavelength ( $\lambda_n$ ) of ISO as a function of the carrier concentration (N) in comparison to ITO. The intrinsic *N* of TCOs is typically controllable through the manipulation of the oxygen vacancy and dopant concentrations between 10<sup>19</sup> to 10<sup>21</sup> cm<sup>-3</sup> [39]. Compared with ITO, ISO demonstrates wider tunability of the plasma wavelength, thus extending the ENZ modulation to longer wavelengths.

# 2.3 Reflectance characterization and analysis

The three-dimensional (3D) finite element method (FEM) was used to calculate the reflectance spectrum

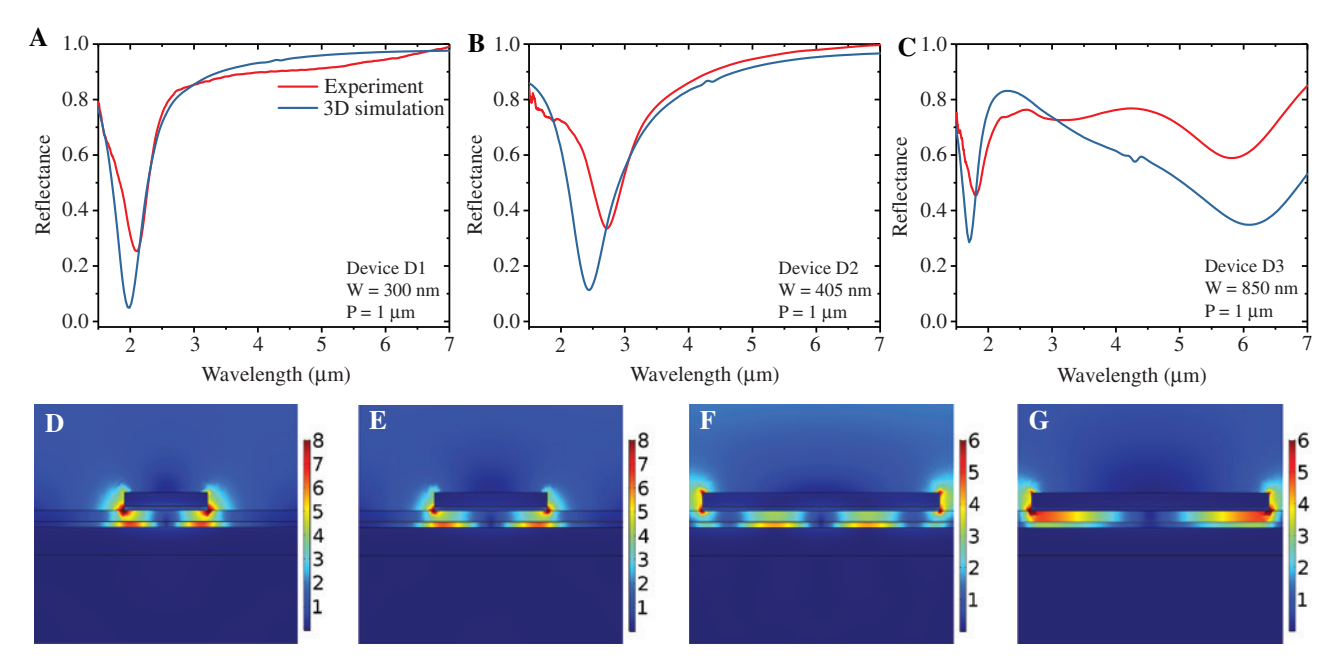


Figure 6: The simulations by 3D finite element method.

(A-C) Comparison of the simulations and experimental FTIR reflectance measurements for devices D1, D2 and D3. (D) Electric field profile of device D1 calculated at  $\lambda = 2.0 \, \mu m$ . (E) Electric field profile of device D2 calculated at  $\lambda = 2.45 \, \mu m$ . (F, G) The electric field profiles of device D3 calculated at  $\lambda = 1.70 \ \mu m$  and  $\lambda = 6.05 \ \mu m$ .

of the fabricated ISO metafilm absorber. Measured dispersion data were used for the ISO films [37] and the material dispersion data for Au, Ti, and HfO, were taken from references [40] and [41], respectively. We used tetrahedral meshing with a maximum element size 50 nm and a minimum element size of 2 nm. The degrees-offreedom in our simulations of plasmonic gratings with different widths were approximately 106. Figure 5 shows the simulated unbiased reflectance plotted in a color map. By fixing the grating period to 1 μm, two clear reflectance dip regions were observed as a function of the grating width W and of the incident wavelength. Moreover, we can clearly distinguish two regions of the parameter space wherein the reflectance simulations feature a single dip (W from 150 nm up to 600 nm) or double dips (W larger than 600 nm). Figure 5 also displays the resonant wavelength positions of the devices D1, D2 and D3.

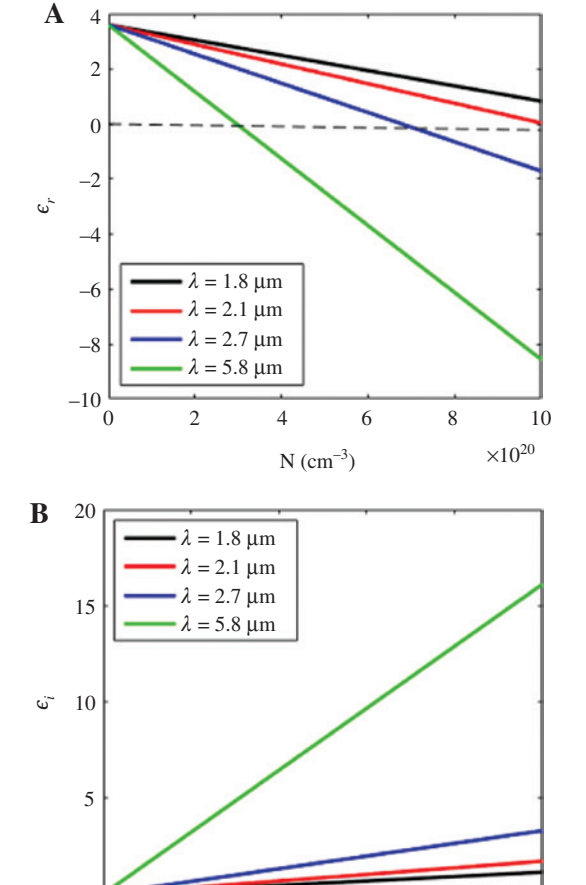


Figure 7: The permittivities of the ISO thin film at the wavelengths of 1.8, 2.1, 2.7 and 5.8 μm.

 $N (cm^{-3})$ 

8

10

 $\times 10^{20}$ 

(A) Real part of the permittivity. (B) Imaginary part of the permittivity.

The reflectance spectra were measured with a Fourier Transform Infrared (FTIR, Bruker VERTEX 70) spectrometer coupled to a  $36 \times$  objective (N.A. 0.5) microscope. The reflected light was detected by a liquid-nitrogen-cooled mercury-cadmium telluride (MCT) detector. A clean Au substrate was used as a reference.

Figure 6 compares the measured reflectance with respect to the simulated reflectance spectra of D1 (panel A), D2 (panel B) and D3 (panel C). The simulation and experimental results qualitatively matched with the dip positions in all the studied configurations. However, the simulated results showed lower amplitude than the experimental results. This can be attributed to the fabrication imperfections, the effect of unintentional annealing (e.g. resist baking) that can slightly modify the material dispersion [37] and the non-perfect normal incidence during the measurements. Figure 6D and E show the calculated field profiles at the cavity resonance wavelengths for D1 and D2,

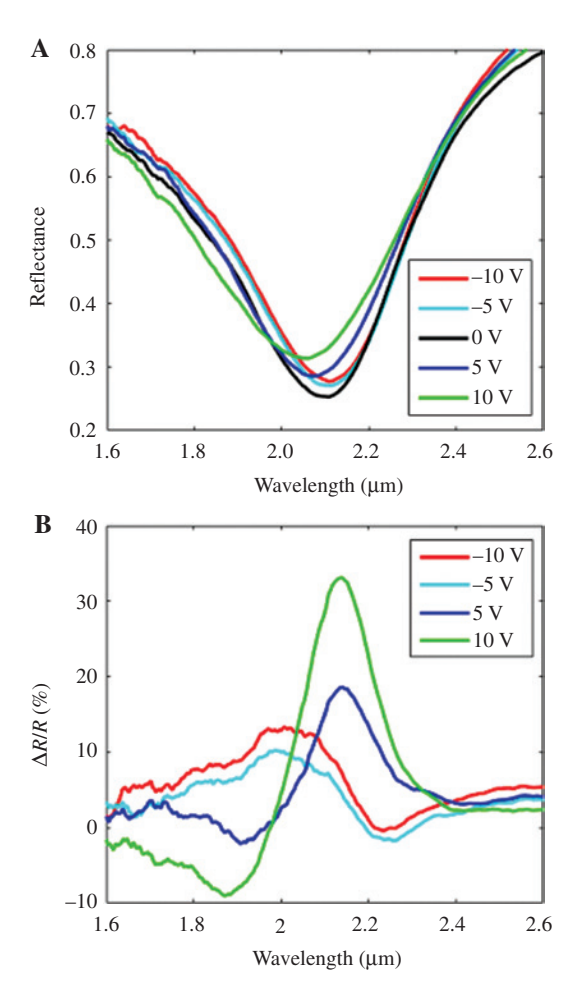


Figure 8: The experimental demonstration of the active tuning for device D1 (P=1.0  $\mu$ m, W=300 nm). (A) Measured reflectance spectra. (B) Relative reflectance change:  $\Delta R/R = [R(V) - R(0)]/R(0).$ 

respectively. They both show strong field enhancements localized on a sub-wavelength scale in the ISO layer. Figure 6F and G display the field distributions at the two cavity resonance wavelengths of D3. The mode profile at the shorter resonance wavelength showed field enhancement in the ISO layer, whereas the field distribution at the longer resonance wavelength was mostly concentrated inside the HfO, layer. The larger imaginary permittivity of ISO at the longer resonance wavelength resulted in a broader reflectance dip consistent with the calculated reduction of the field amplitude in the ISO at this wavelength.

From the measured reflectance spectra for D1, D2 and D3, the resonance dips were observed at the wavelengths of 2.1, 2.7, 1.8 and 5.8 μm, respectively. The permittivities of the ISO thin film at the above wavelengths are plotted in Figure 7. At the wavelength of 5.8  $\mu$ m,  $\varepsilon_{\star}$ equals to zero as N was around 2.96 × 10<sup>20</sup> cm<sup>-3</sup>, close to the measured carrier concentration of the ISO layer in this work.

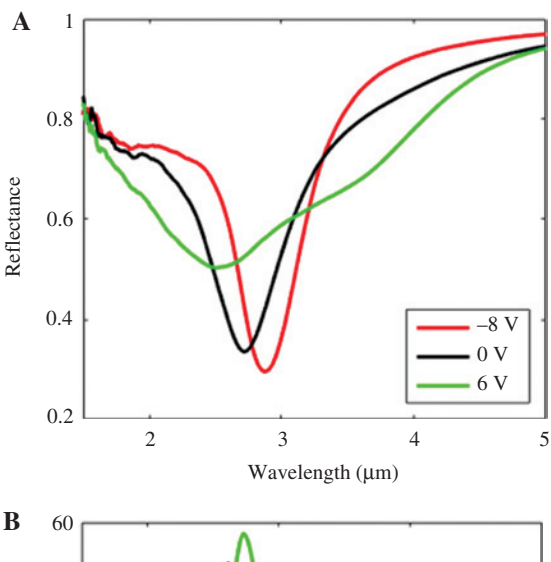
## 3 Gate-tunable measurement

A gate bias was applied to the metallic grating arrays using the larger contact pads while the reflecting substrate was connected to the ground. The carrier concentration near the ISO/HfO<sub>2</sub> interface increases or decreases by forming a carrier accumulation or depletion layer. The permittivity of the accumulation/depletion layer inside the ISO is tuned with the gate bias, resulting in the modulation of the reflected light.

The reflectance spectra of D1 for the applied biases of -10, -5, 0, +5, and +10 V are shown in Figure 8A. The resonance wavelength shifted by -50 nm with a +10 V bias. Figure 8B shows the relative reflectance change,  $\Delta R/R = [R(V) - R(0)]/R(0)$ , defined as the normalized ratio of the change in reflectance with and without bias. For D1, a reflectance change of up to 33% was demonstrated at a wavelength of 2.14 µm with a bias of +10 V.

The measured reflectance spectra and relative reflection change for device D2 and D3 are shown in Figures 9 and 10, respectively. A maximum  $\Delta R/R$  of 57% was measured for device D2 at a wavelength of 2.73 um with a bias of 6 V and the resonance wavelength shift was -216 nm. With a bias of -8 V, the resonance wavelength shift was +150 nm and  $\Delta R/R$  was 50% at a wavelength of  $2.6 \,\mu m$ .

Two resonances, located at 1.807 µm and 5.801 µm, respectively, were observed for device D3 in the region of



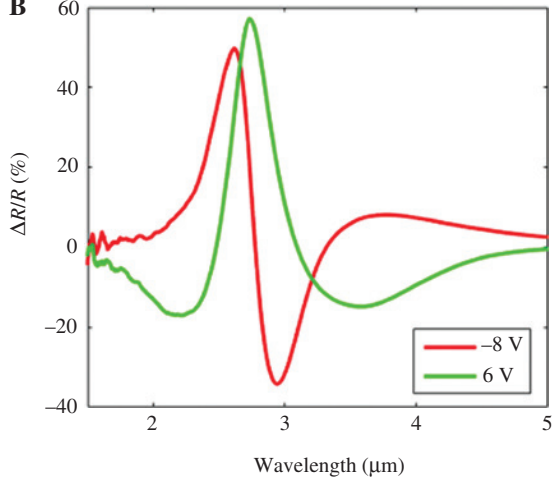
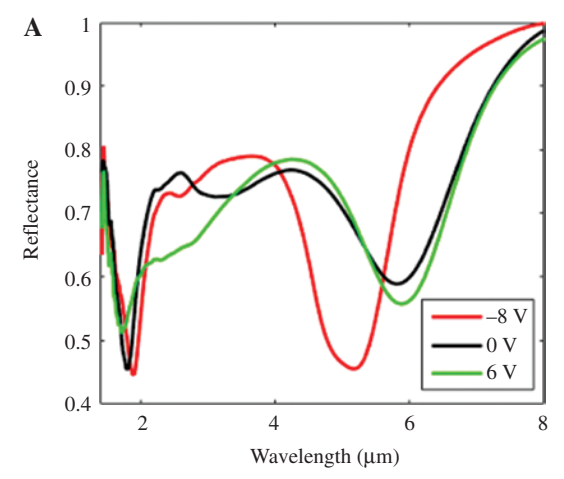


Figure 9: The experimental demonstration of the active tuning for device D2 (P=1.0  $\mu$ m, W=405 nm).

(A) Measured reflectance spectra. (B) Relative reflectance change.

observed operation. At a bias of -8 V, the two resonances were shifted to 1.895 µm and 5.175 µm, resulting in a +80 nm and -620 nm shift, respectively. Figure 10 displays larger resonance wavelength shift and  $\Delta R/R$  values at the longer wavelength resonance. This is consistent with the expectation of modulation enhancement around the ENZ wavelength.

These results for the ISO-based metafilm absorber compare favorably to other materials, thereby showing promise for widely applicable gate-tunable metasurface devices. Such gate-tunable devices enable electrically addressing the individual subwavelength resonator elements. The obtained large resonance shift can be further investigated to realize the phased arrays of the subwavelength resonators for flat optical elements, LIDAR and beam steering/pointing in free space optical communications.



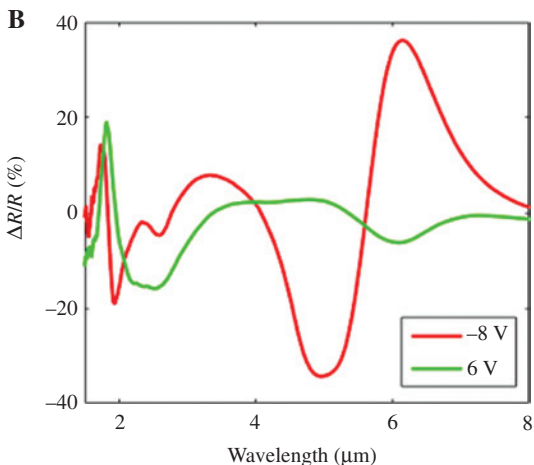


Figure 10: The experimental demonstration of active tuning for device D3 (P=1.0  $\mu$ m, W=850 nm). (A) Measured reflectance spectra. (B) Relative reflectance change.

# 4 Conclusions

We have demonstrated tunable metafilm absorbers based on ISO. Three devices with different geometries were fabricated and characterized. The light reflectance was tuned with a gate bias applied between the metallic resonator and the reflecting substrate. A reflectance change of 57% was measured at a wavelength of 2.73 µm, and the maximum resonance wavelength shift of 620 nm was realized with a bias of -8 V. These promising results, to our knowledge, represent the first demonstration of gatetunable metafilm absorbers based on ISO. Future efforts will be made to investigate high-speed optical modulation; and to study the active phase tuning in individual resonator elements towards reconfigurable beam steering applications.

**Acknowledgment:** Portions of this work were supported by the National Science Foundation (NSF DMR #1709704,

Funder Id: http://dx.doi.org/10.13039/100000001) and the Air Force Office of Scientific Research (FA 9550-16-1-0393, Funder Id: http://dx.doi.org/10.13039/100006831).

# References

- [1] Polman A, Atwater HA. Plasmonics: optics at the nanoscale. Mater Today 2005;8:56.
- [2] Pors A, Bozhevolnyi SI. Plasmonic metasurfaces for efficient phase control in reflection. Opt Express 2013;21:27438-51.
- [3] Chen H, Taylor AJ, Yu N. A review of metasurfaces: physics and applications. Rep Prog Phys 2016;79:076401.
- [4] Falcone F, Lopetegi T, Laso M, et al. Babinet principle applied to the design of metasurfaces and metamaterials. Phys Rev Lett 2004;93:197401.
- [5] Yu N, Genevet P, Aieta F, et al. Flat optics: controlling wavefronts with optical antenna metasurfaces. IEEE J Sel Top Quantum Electron 2013;19:4700423.
- [6] Aieta F, Genevet P, Yu N, Kats MA, Gaburro Z, Capasso F. Outof-plane reflection and refraction of light by anisotropic optical antenna metasurfaces with phase discontinuities. Nano Lett 2012;12:1702-6.
- [7] Lee HW, Papadakis G, Burgos SP, et al. Nanoscale conducting oxide plasmostor. Nano Lett 2014;14:6463-8.
- [8] Azad AK, Kort-Kamp WJ, Sykora M, et al. Metasurface broadband solar absorber. Sci Rep 2016;6:20347.
- [9] Panchenko E, Cadusch JJ, James TD, Roberts A. Plasmonic metasurface-enabled differential photodetectors for broadband optical polarization characterization. ACS Photonics 2016;3:1833-9.
- [10] Zeng S, Sreekanth KV, Shang J, et al. Graphene-gold metasurface architectures for ultrasensitive plasmonic biosensing. Adv Mater 2015;27:6163-9.
- [11] Iyer PP, Pendharkar M, Palmstrøm CJ, Schuller JA. Ultrawide thermal free-carrier tuning of dielectric antennas coupled to epsilon-near-zero substrates. Nat Commun 2017;8:472.
- [12] Zhao YT, Wu B, Huang BJ, Cheng Q. Switchable broadband terahertz absorber/reflector enabled by hybrid graphene-gold metasurface. Opt Express 2017;25:7161-9.
- [13] Babicheva VE, Kinsey N, Naik GV, et al. Towards CMOS-compatible nanophotonics: ultra-compact modulators using alternative plasmonic materials. Opt Express 2013;21:27326-37.
- [14] Iyer PP, Pendharkar M, Schuller JA. Electrically reconfigurable metasurfaces using heterojunction resonators. Adv Opt Mater 2016;4:1582-8.
- [15] Naik GV, Shalaev VM, Boltasseva A. Alternative plasmonic materials: beyond gold and silver. Adv Mater 2013;25:3264-94.
- Jun YC, Reno J, Ribaudo T, et al. Epsilon-near-zero strong coupling in metamaterial-semiconductor hybrid structures. Nano Lett 2013;13:5391-6.
- [17] Iyer PP, DeCrescent RA, Lewi T, Antonellis N, Schuller JA. Uniform thermo-optic tunability of dielectric metalenses. Phys Rev Appl 2018;10:044029.
- [18] Iyer PP, Pendharkar M, Palmstrøm CJ, Schuller JA. III-V heterojunction platform for electrically reconfigurable dielectric metasurfaces. ACS Photonics 2019;6:1345-50.
- [19] Yi F, Shim A, Zhu AY, Zhu H, Reed JC, Cubukcu E. Voltage tuning of plasmonic absorbers by indium tin oxide. Appl Phys Lett 2013;102:221102.

- [20] Liu X, Park J, Kang J-H, et al. Quantification and impact of nonparabolicity of the conduction band of indium tin oxide on its plasmonic properties. Appl Phys Lett 2014;105:181117.
- [21] Zhao H, Wang Y, Capretti A, Dal Negro L, Klamkin J. Broadband electroabsorption modulators design based on epsilonnear-zero indium tin oxide. IEEE J Sel Top Quantum Electron 2015;21:192-8.
- [22] Wang Y, Overvig AC, Shrestha S, et al. Tunability of indium tin oxide materials for mid-infrared plasmonics applications. Opt Mater Express 2017;7:2727-39.
- [23] Morea M, Zang K, Kamins TI, Brongersma ML, Harris JS. Electrically tunable, cmos-compatible metamaterial based on semiconductor nanopillars. ACS Photonics 2018;5:4702-9.
- [24] Kim J, Naik GV, Gavrilenko AV, et al. Optical properties of gallium-doped zinc oxide - a low-loss plasmonic material: firstprinciples theory and experiment. Phys Rev X 2013;3:041037.
- [25] Pradhan A, Mundle R, Santiago K, et al. Extreme tunability in aluminum doped zinc oxide plasmonic materials for near-infrared applications. Sci Rep 2014;4:6415.
- [26] Huang Y-W, Lee HWH, Sokhoyan R, et al. Gate-tunable conducting oxide metasurfaces. Nano Lett 2016;16:5319-25.
- [27] Park J, Kang J-H, Liu X, Brongersma ML. Electrically tunable epsilon-near-zero (ENZ) metafilm absorbers. Sci Rep 2015;5:15754.
- [28] Park J, Kang J-H, Kim SJ, Liu X, Brongersma ML. Dynamic reflection phase and polarization control in metasurfaces. Nano Lett 2016;17:407-13.
- [29] Butakov NA, Knight MW, Lewi T, et al. Broadband electrically tunable dielectric resonators using metal-insulator transitions. ACS Photonics 2018;5:4056-60.
- [30] Kafaie Shirmanesh G, Sokhoyan R, Pala RA, Atwater HA. Dualgated active metasurface at 1550 nm with wide (>300°) phase tunability. Nano Lett 2018;18:2957-63.

- [31] Liu X, Kang J-H, Yuan H, et al. Electrical tuning of a quantum plasmonic resonance. Nat Nanotechnol 2017;12:866.
- [32] Mitoma N, Da B, Yoshikawa H, et al. Phase transitions from semiconductive amorphous to conductive polycrystalline in indium silicon oxide thin films. Appl Phys Lett 2016;109:221903.
- [33] Lee H-M, Kang S-B, Chung K-B, Kim H-K. Transparent and flexible amorphous In-Si-O films for flexible organic solar cells. Appl Phys Lett 2013;102:021914.
- [34] Mitoma N, Aikawa S, Gao X, et al. Stable amorphous In<sub>2</sub>O<sub>2</sub>based thin-film transistors by incorporating SiO, to suppress oxygen vacancies. Appl Phys Lett 2014;104:102103.
- [35] Aikawa S, Nabatame T, Tsukagoshi K. Effects of dopants in InO<sub>2</sub>based amorphous oxide semiconductors for thin-film transistor applications. Appl Phys Lett 2013;103:172105.
- [36] Maruyama T, Tago T. Germanium-and silicon-doped indiumoxide thin films prepared by radio-frequency magnetron sputtering. Appl Phys Lett 1994;64:1395-7.
- [37] Britton W, Zhang R, Shrestha S, Chen Y, Yu N, Dal Negro L. Indium silicon oxide thin films for infrared metaphotonics. Appl Phys Lett 2019;114:161105.
- [38] Zhao H, Zhang R, Chorsi HT, et al. Tunable metasurface based on silicon doped indium oxide. Proc. Advanced Photonics Congress (BGPP, IPR, NP, NOMA, Sensors, Networks, SPPCom, SOF). 2019:NoTh3B.6.
- [39] Feigenbaum E, Diest K, Atwater HA. Unity-order index change in transparent conducting oxides at visible frequencies. Nano Lett 2010;10:2111-6.
- [40] Palik ED. Handbook of optical constants of solids. Maryland Heights, MO, USA, Elsevier, 1998;3.
- [41] Kruschwitz JDT, Pawlewicz WT. Optical and durability properties of infrared transmitting thin films. Appl Opt 1997;36:2157-9.